

Two-Dimensional Characterization of Microwave E-fields and Beam Profiles of the ECR Ion Thruster $\mu 20$

IEPC-2007-25

*Presented at the 30th International Electric Propulsion Conference, Florence, Italy
September 17-20, 2007*

Kazutaka Nishiyama* and Hitoshi Kuninaka†
*Japan Aerospace Exploration Agency / Institute of Space and Astronautical Science,
Sagamihara, Kanagawa, 229-8510, Japan*

and

Tatsuya Nakai‡
The University of Tokyo, Bunkyo-ku, Tokyo, 113-8656, Japan

Abstract: A 20-cm diameter ECR ion thruster “ $\mu 20$ ” is equipped with unique magnet and gas injector layout that maximize thruster performance. We have experimentally investigated two-dimensional microwave E-field distributions inside the discharge chamber under beam extraction and beam profiles 5-cm downstream the ion optics. The distributions were quite different between the best and the worst gas injector configurations. All the parameters in the worst case showed very uniform distributions. On the other hand, the best case showed obvious peaks of both the E-field and the beam current density. It turned out that, in the best configuration, microwave reflection was sufficiently small (less than 10%) and 70 – 90% of the microwave power launched into the discharge chamber is absorbed by plasma electrons with less direct heating of the discharge chamber walls. Generally, the non-uniform plasma is not preferable to design ion optics. However, the performance advantage of the non-uniform discharge is not negligible as for this ion thruster. We have decided to accept the best configuration and to cope with the plasma non-uniformity by changing aperture diameters of the accelerator electrode by the place aiming increase of the propellant utilization efficiency. Promising performance test results have been obtained using a newly fabricated small hole accelerator grid, though large accelerator currents are still observed due to ion beam direct impingement. Ion machining of the grid has just started to determine the best accelerator grid hole geometries.

I. Introduction

In order to advance the technology of the cathode-less microwave discharge ion engines known as the “ μ ” family, two programs are currently under development: $\mu 20$ and $\mu 10$ HIsp. The former is a 20-cm diameter microwave discharge ion engine, and the latter is a higher specific impulse version of the 10-cm diameter $\mu 10$. Table I summarizes the performance of the three μ models. The goal of R&D on $\mu 20$ is to achieve 30 mN/kW in the thrust-to-power ratio. The $\mu 10$ system is capable of generating 140 mA ion beam current with 32 W microwave power, yielding ion production cost of 230 W/A. This production cost is within average value of 10-cm class ion

* Associate Professor, Space Transportation Division, nishiyama@ep.isas.jaxa.jp.

† Professor, Space Transportation Division, kuninaka@isas.jaxa.jp.

‡ Graduate Student, Department of Aeronautics and Astronautics, School of Engineering, nakai@ep.isas.jaxa.jp.

sources. However, due to the low conversion efficiency of the microwave generator, the total efficiency and the thrust-to-power ratio are inferior to those of the electron bombardment type ion thrusters. The $\mu 20$ system aims to generate ions at about 200 W/A production cost. The target thrust-to-power ratio can be achieved with optimization of the microwave network. The highly biased ion source of the electron bombardment ion thruster is fed power, command and telemetry through isolation transformers and/or optical equipment, which are sensitive and weighty components. The μ technology eliminates these isolations because the ion source includes no active electronics devices as illustrated in Figure 1. Magnetic field and propellant injection method of the ion source have been optimized. The performance is deemed to be highly dependent on the propellant injection method. Though specific impulse and propellant utilization efficiency still remain conservative, the main goal of increasing the thrust-to-power ratio from 22 mN/kW of $\mu 10$ to 30 mN/kW of $\mu 20$ had been almost accomplished as reported in a former publication¹. After the replacement of the microwave antenna to another model with higher temperature tolerance, the up-to-date thruster performance is shown in Figures 2 and 3. The optimal xenon flow rate that maximize ion beam current and minimize ion production cost at a given microwave power is 10 – 11 standard cubic centimeters per minute (SCCM). In this flow rate range, the propellant utilization efficiency is 0.7 – 0.8. The performance is superior to the worst case with different gas injectors as shown in Figure 4. In this work, we have experimentally investigated two-dimensional microwave E-field distributions inside the discharge chamber under beam extraction and beam profiles 5-cm downstream the ion optics of both injector layouts for better understanding of the performance difference. Trial of improvement of the propellant utilization by employing smaller accelerator grid apertures has just started based on the measured ion beam profile and preliminary results of beam extraction test using a new accelerator grid will also be reported.

II. Experimental Apparatus

The magnetic field and magnet arrangement for $\mu 20$ are illustrated in Figure 5. The distance between the magnet rows is very similar to the one for the $\mu 10$ with the only difference being the prolonged gap for the innermost magnet row. The innermost magnet rows are spaced almost twice as far as the other three rows. This design helps microwave propagate to the outer ECR regions without being disturbed by the dense plasma production around the inner ECR regions. The two radial magnetic bridges between the second and the fourth rows counted from the center, shown in Figure 5, support the transport of high-energy electrons between the inner and outer discharge regions by $E \times B$ drift or grad B ($B \times \nabla B$) drift. With this magnet arrangement, two crescent shaped plasma rings were produced at the same time as shown in Figures 6 and 7. Figure 5 also shows the locations of the gas ports on the yoke (end plate) and some of more than 10 combinations tested. All the ports are cylinders 5-mm in diameter and 5-mm in length. The propellant was injected downstream in parallel to the thruster center axis. Beam currents at the same discharge power and the flow rate differ 20% at maximum for the best and the worst gas-injector layouts as shown in Figures 3 and 4. The total mass flow rate of xenon was controlled with a single controller, and the propellant feeders were evenly divided before being connected to the ports. The exact distribution ratios were not measured. There were several valves in the feed lines so the gas distribution pattern can be quickly changed while maintaining the operation of the thruster. The vacuum pressures in the test chamber were 6.0×10^{-5} Pa without load and 1.0×10^{-3} Pa with 10 SCCM xenon flow. The beam extraction was carried out with a screen voltage of 1100 V and an accelerator voltage of -350 V. The decelerator was not biased. No neutralizer was used. Grid thicknesses are 0.75 mm for the screen grid and 1.0 mm for both the accelerator grid and the decelerator grid. Grid separations are 0.7 mm between the screen and accelerator and 0.20 mm between the accelerator and decelerator.

Forward and reflected microwave powers were always monitored by the amplifier. Taking calibrated RF cable losses into account, forward and reflected powers at the antenna connector can be calculated. The thruster performances are based on the powers defined at this electrical interface because cable losses or power conversion efficiencies of a flight model of the microwave power supply unit are unknown. Unless otherwise specified, “microwave power” contains microwave power reflected back to the amplifier. We will use another term “net microwave power” that is a power actually consumed inside the ion source discharge chamber. The reflected power will be subtracted from the “microwave power” to obtain the “net microwave power”. From the propulsion system point of view, “microwave power” is important, while “net microwave power” is still important from the plasma physics viewpoint.

Semi-rigid type electric probes were used to measure the electric field at discharge chamber inner surfaces between magnets. This probe has a SMA type coaxial connector in one end. Another end is a center conductor stripped by 5 mm. Nine probes were installed to the thruster at a time. Received microwave signals were transmitted by way of flexible coaxial cables and vacuum feedthroughs. A pair of DC-block and crystal detector was used to

measure the signal intensity by reconnecting it to one probe after another in atmosphere by hand. Total number of measurement positions was 48 and 6 times of experimental sequences (probe setting, evacuation, measurement and vacuum break) were required. All the RF components were well calibrated at the ECR discharge frequency of 4.25 GHz except for “antenna gain” of the probes. Actually, the absolute value of the E-field intensity is not so important in this work. Relative gain difference between 9 probes are supposed to be negligibly small so that reasonable E-field distribution can be measured.

Ion beam profile was measured with a 1-mm diameter tungsten probes located at 5-cm downstream from the decelerator grid. An array of twenty-nine probes were traversed at the same time. The gap between probes are 5 mm. This array can move in one direction (x) and can rotate around the thruster center axis (z). Three sweeps of the array with different angles can cover the entire beam area. To repel electrons, biased voltage of -50 V was applied to all the probes. Thus we obtained current density data every 5 mm in both x and y directions. The total current integrated in the whole beam area seems approximately 40% larger than the thruster beam current. We have normalized the raw data so that the surface integral of the current density equals the beam current.

Table 1. Performance of “μ” series ion thrusters.

Items	μ10 (achi eved)	μ20 (target)	μ10HIsp (target)
Ion Prod. Cost (W/A)	230	200	230
Beam Current (mA)	140	500	140
μw Power (W)	32	100	32
Screen Voltage (V)	1,500	1,100	15,000
Specific Imp. (s)	3,000	2,800	10,000
Thrust (mN)	8.5	27	27
System Power (W)	350	900	2,500
Thrust/Power (mN/kW)	22	30	11

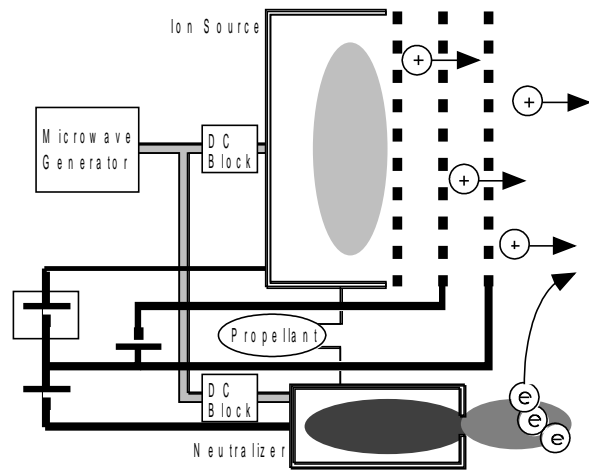


Figure 1. System configuration of microwave discharge ion thruster.

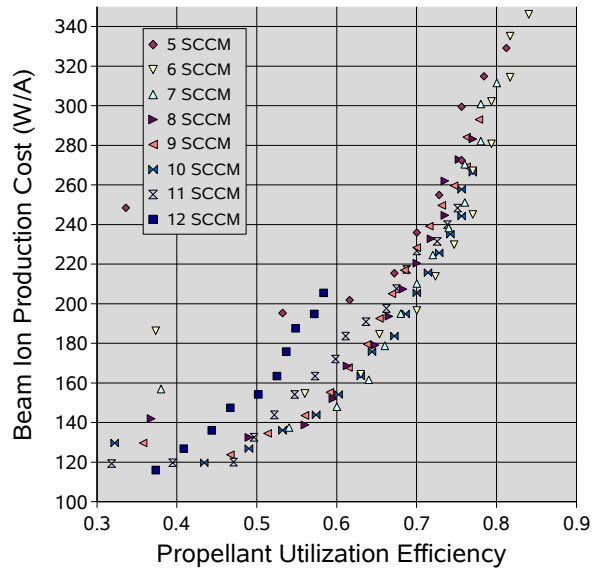


Figure 2. Beam ion production cost as a function of propellant utilization efficiency of the best injector layout.

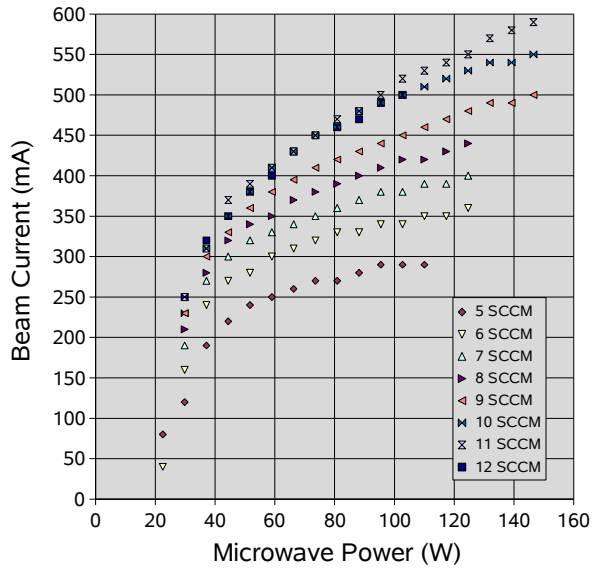


Figure 3. Ion beam current as a function of microwave power with the best injector layout.

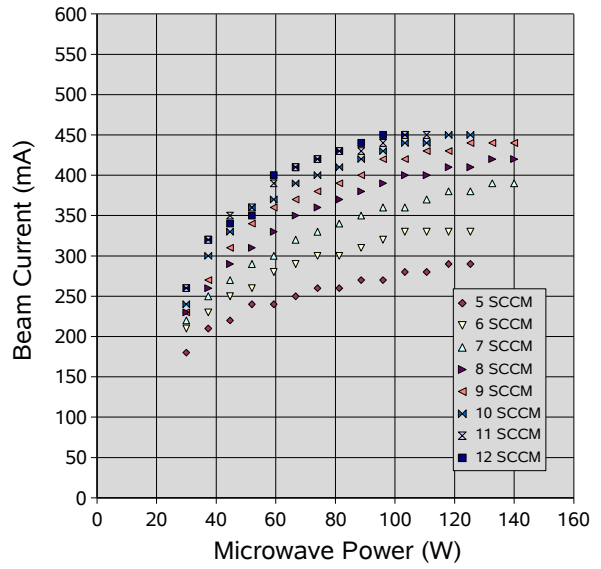


Figure 4. Ion beam current as a function of microwave power with the worst injector layout.

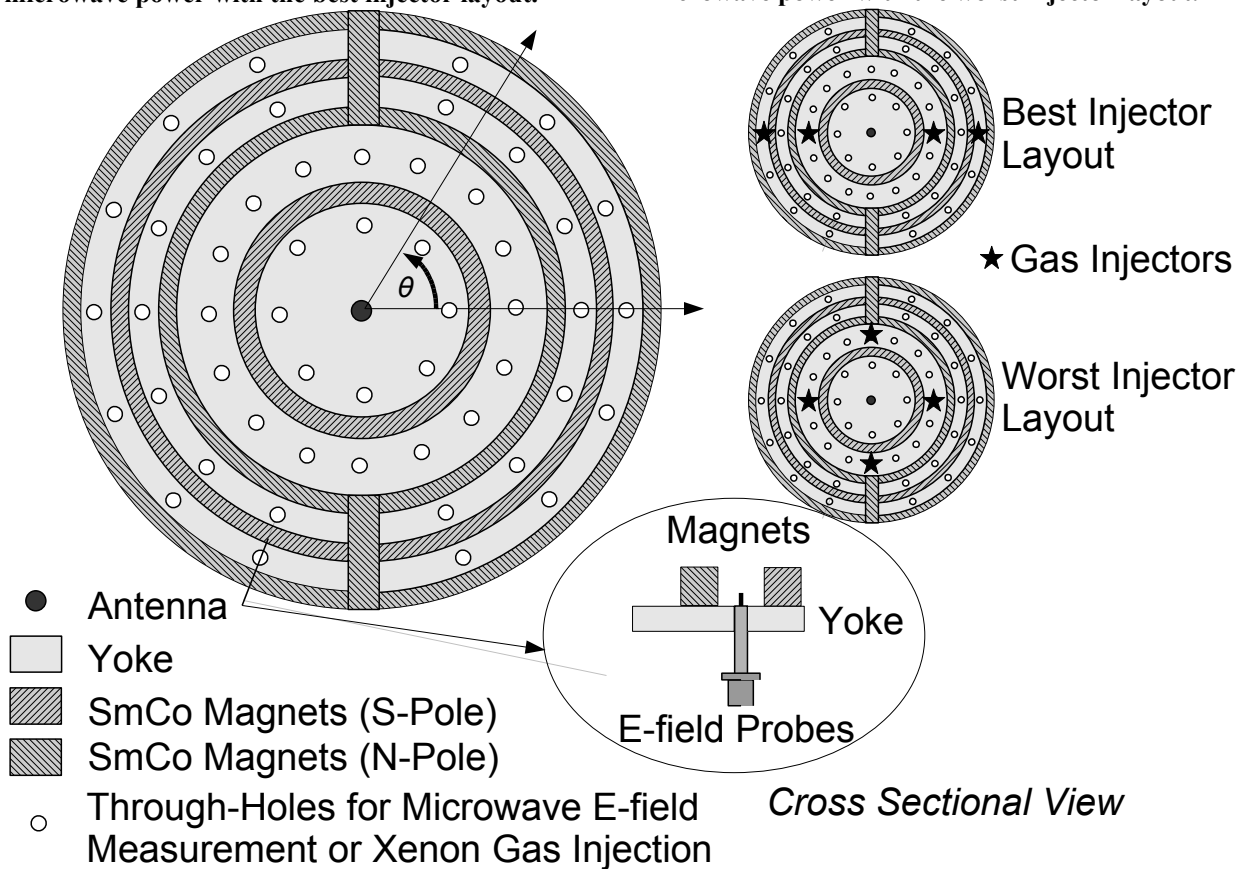


Figure 5. Layout of magnets and propellant ports (Cross sectional front view of the flat discharge chamber).

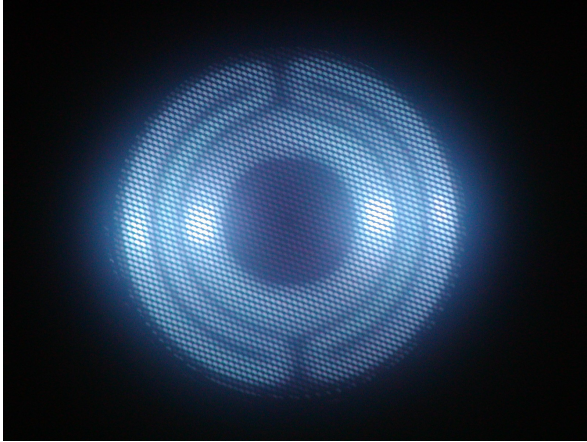


Figure 6. Front view of the operating $\mu 20$ with the best injector layout. Four luminous spots correspond to gas injector locations.

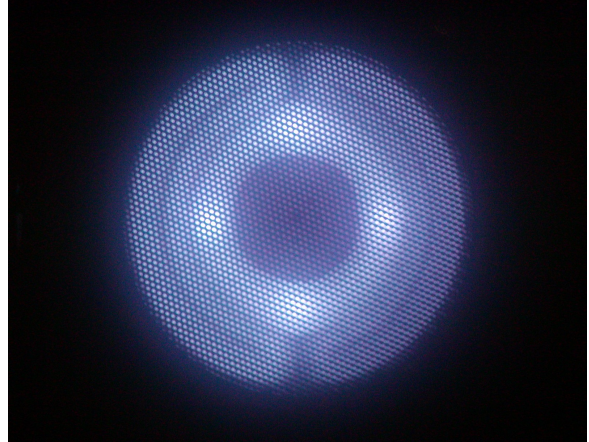


Figure 7. Front view of the operating $\mu 20$ with the worst injector layout. Four luminous spots correspond to gas injector locations.

III. Results and Discussions

A. Microwave E-field Distribution

Figure 8 shows a two-dimensional microwave E-field distribution at a nominal thrust level. Field intensities are shown in dB values relative to the net microwave power. The detected powers vary three orders of magnitude (30 dB) by locations and azimuthal non-uniformity is clearly observed. It is difficult to identify any simple symmetry axes. Figure 9 is another expression of the same data as Figure 8. E-field is the strongest at the inner most measurement positions of all the measured radial positions. Generally speaking, the larger the radial position is, the weaker the E-field strength. There are two peaks along the azimuthal direction and intensity variation reaches one to two orders of magnitude. Figure 10 shows a distribution at a small thrust level. Although number of peaks remains two, the peak azimuthal angles are slightly shifted from the positions observed in Figure 9. Intensity modulation along the azimuthal direction in Figure 10 is slightly weaker than in Figure 9. Figure 11 shows a distribution when the xenon gas was injected from “the worst layout” gas ports. Obvious peaks can not be seen. Without plasma discharge, the E-field distribution shown in Figure 12 has three peaks along the azimuthal direction.

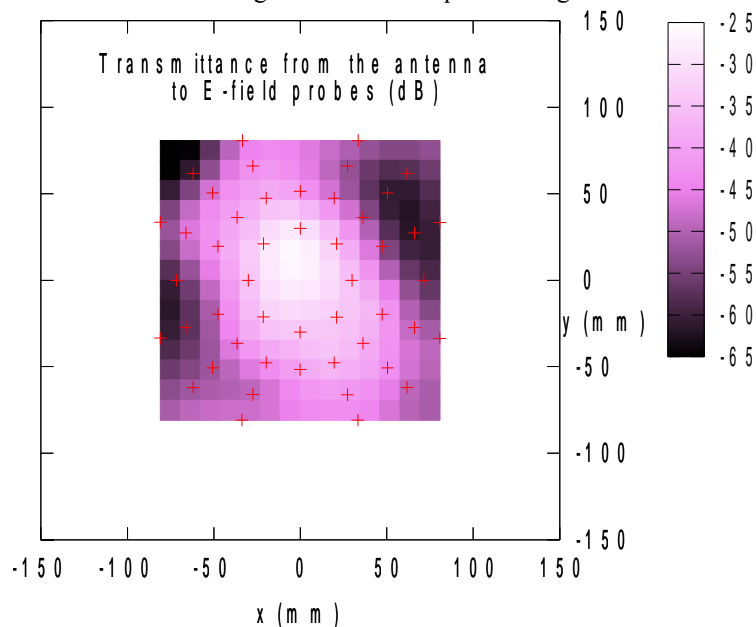


Figure 8. Two-dimensional microwave E-field distribution. (10 SCCM, 94(= 102 - 8) W, 500 mA) Intensities are shown in dB values relative to the net microwave power. Red crosses indicate 48 measurement points.

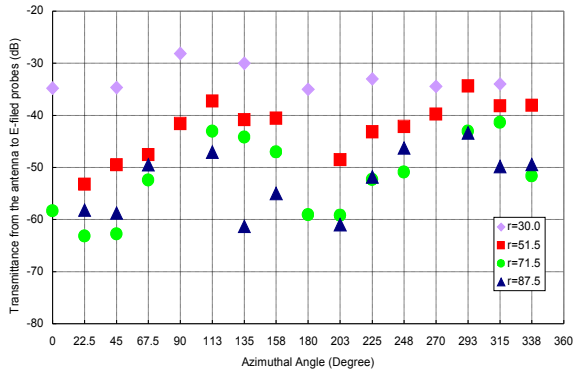


Figure 9. Microwave E-field distributions of the best injector layout. (10 SCCM, 94(= 102 - 8) W, 500 mA)

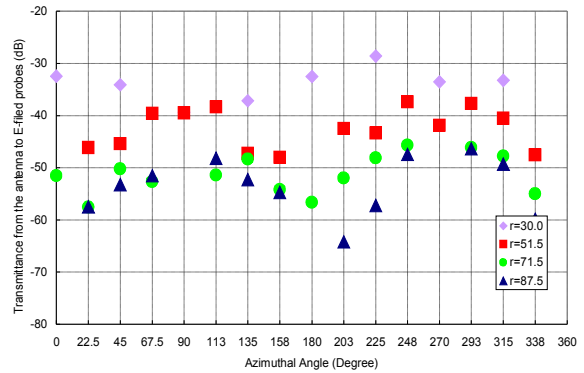


Figure 10. Microwave E-field distributions of the best injector layout. (5 SCCM, 89(= 103 - 14) W, 290 mA)

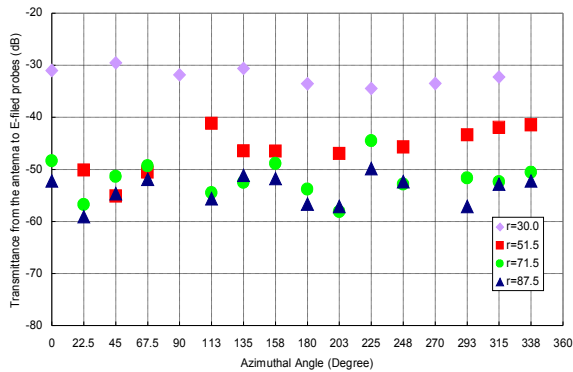


Figure 11. Microwave E-field distributions of the worst injector layout. (10 SCCM, 73(= 103 - 30) W, 430 mA)

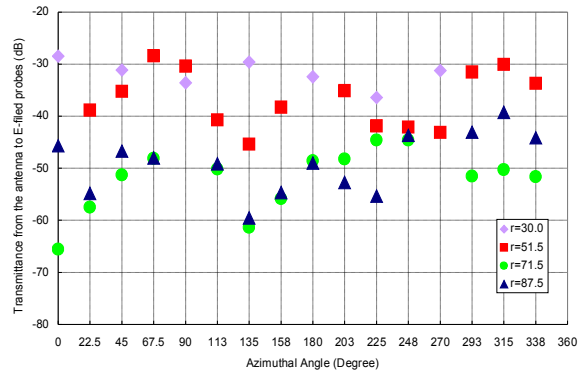


Figure 12. Microwave E-field distributions without plasma discharge in vacuum. (0 SCCM, 17(= 44 - 27) W)

B. Microwave Power Absorption Coefficient

By integrating the data like Figures 9 – 12, direct wall heating by microwaves can be roughly estimated. The Joule heating of the discharge chamber wall surfaces is one of discharge loss mechanism specific to ECR ion thrusters. Of course, it is impossible to measure the E-fields at all the inner surfaces. However, interpolating limited locations of measured data or assuming the symmetry of the distribution on the grid surfaces to the one on the end wall (magnets and the yoke), we can compare the total Joule heatings inside the discharge chamber with and without plasma discharge. Integration was conducted by considering chamber wall surface areas around the probes so that outer probes have more contribution to the power dissipation than inner ones. Figure 13 shows the integrated E-field detector powers in arbitrary unit as a function of the net microwave power. The integrated powers are the largest without plasma. In this case, all the microwave powers are consumed for the wall heating. When discharge plasma exists, most of the net microwave powers are consumed for plasma electron heating and rest of them are dissipated to the wall surfaces. Thus the integrated E-field detector powers with plasma are much smaller than without plasma. As increasing the net microwave power, Joule heating of the wall surfaces also increases. There are some threshold microwave powers where the increasing rate of the Joule heating becomes larger. This suggests saturation of the microwave absorption by plasma electrons as the electron density gets close to a critical density which is so called “cut-off” density. Figure 13 can be translated into Figure 14 that shows microwave absorption coefficient as a function of the net microwave power. This coefficient indicates the fraction of microwave powers absorbed by electrons to all the microwave powers launched into the discharge chamber. How to calculate the coefficient is;

$$1 - (\text{Integrated E-filed Detector Power with Plasma}) / (\text{Integrated E-filed Detector Power without Plasma}).$$

The data of integrated E-filed detector power without plasma is limited to low power range because of the limitation of tolerance of the reflected power to the microwave amplifier, and was extrapolated according to the linear curve fit result. Figure 14 shows that the microwave absorption coefficient of the $\mu 20$ ion thruster is 0.7 – 0.9 and probably lower at higher microwave powers. The coefficient decreases as the net microwave power increases.

Note that the coefficient has nothing to do with the power reflection. Even if there is no reflection, the coefficient will never be unity. The reason that the data plot of the worst injector case is compressed to the smaller net microwave power side is that the reflected power is as large as 30% of forward power. The large reflection is the primary cause of the poor performance of the worst injector layout. Another cause will be the lower microwave power absorption coefficient. To overcome the decrease of the microwave absorption coefficient at higher thrust levels, combination of the higher microwave frequency and the stronger magnetic field which increase the critical density will be effective as reported in a former publication².

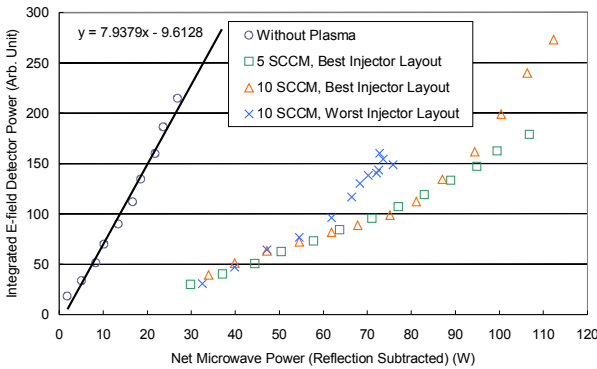


Figure 13. Integrated E-field detector powers as a function of the net microwave power.

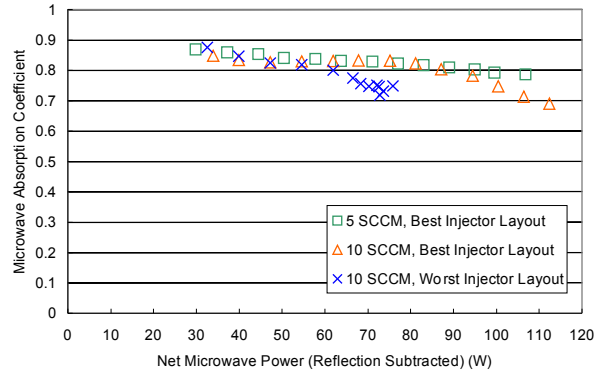


Figure 14. Microwave absorption coefficient as a function of the net microwave power.

C. Beam Profile

Because the discharge chamber geometry is far from axially symmetric, two dimensional beam profile measurement is necessary for thruster characterization. Figures 15 – 17 show the beam current density distributions as increasing the thrust level. There are high density regions near gas injector positions and distributions resemble the photograph of the plasma discharge as shown in Figure 6. Figures 16 and 17 contains small blight spot near the discharge chamber's outer edge, which is probably due to anomalous discharge between the thruster and the probes. The highest current density observed was 3.5 mA/cm². Beam flatness was extremely poor as everyone had expected. Ironically, the beam profile of the worst injector layout shown in Figure 18 has excellent beam flatness. The performance advantage of the non-uniform discharge is not negligible as for this ion thruster as indicated in Figures 3 and 4. We have decided to accept the best injector layout and to cope with the plasma non-uniformity by changing aperture diameters of the accelerator electrode by the place aiming increase of the propellant utilization efficiency.

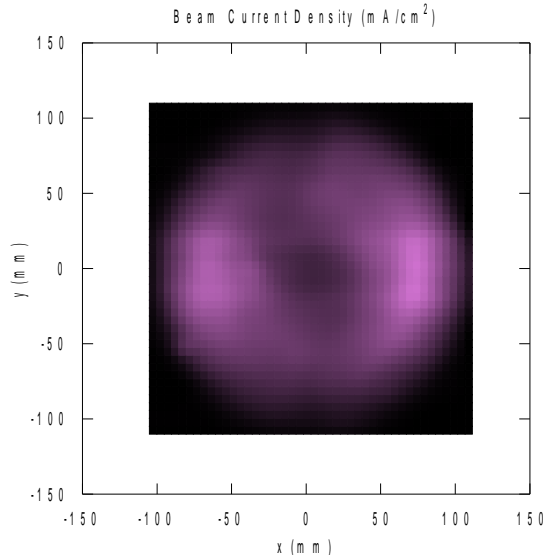


Figure 15. Beam current density profile at a minimum thrust level (5 SCCM, 55 W, 250 mA).

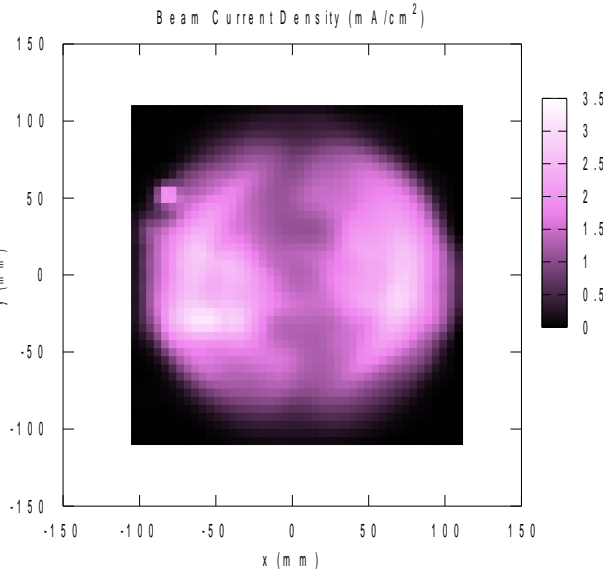


Figure 16. Beam current density profile at a nominal thrust level (10 SCCM, 100 W, 500 mA).

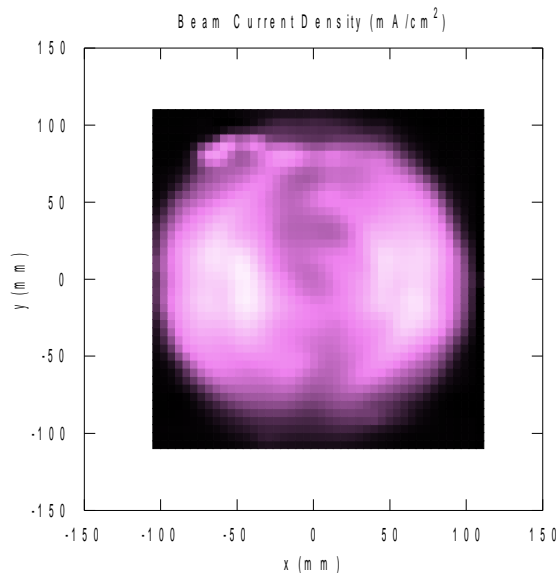


Figure 17. Beam current density profile at a nearly maximum thrust level (12 SCCM, 140 W, 570 mA).

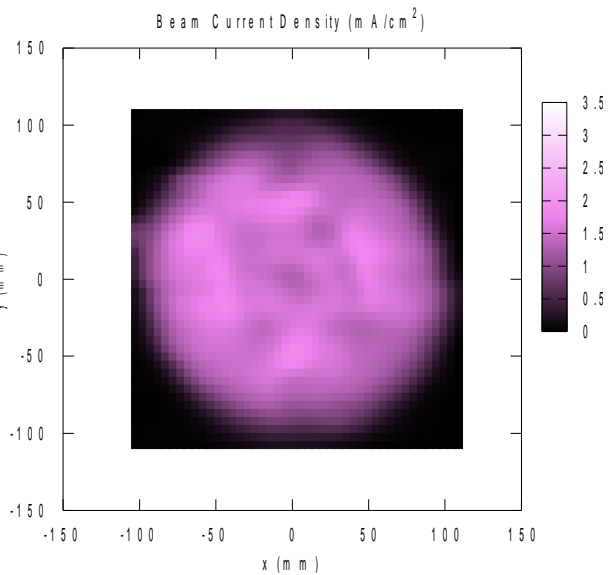


Figure 18. Beam current density profile of the worst injector layout (10 SCCM, 100 W, 430mA).

D. Very Small Hole Accelerator Grid

Referring Figures 15 – 17, a new accelerator grid that is replaceable with the original accelerator grid was designed and fabricated. Its aperture diameter distribution is shown in Figure 19. A two dimensional ion optics code OPT³ was used to determine the aperture diameters. The aperture diameters were much reduced so aggressively from the original value of 1.8 mm that excessive accelerator grid impingement currents were expected. Promising performance test results have been obtained using a the new grid, though accelerator currents as large as 10% of the screen currents are still observed. Screen current as a function of the microwave power is shown in Figure 20. Xenon flow rate was able to reduce from 10 SCCM to 6.5 SCCM in order to generate the same level of screen current, which led to the great improvement in propellant utilization efficiency as shown in Figure 21. Ion machining⁴ of the grid has just started to determine the best accelerator grid hole geometries.

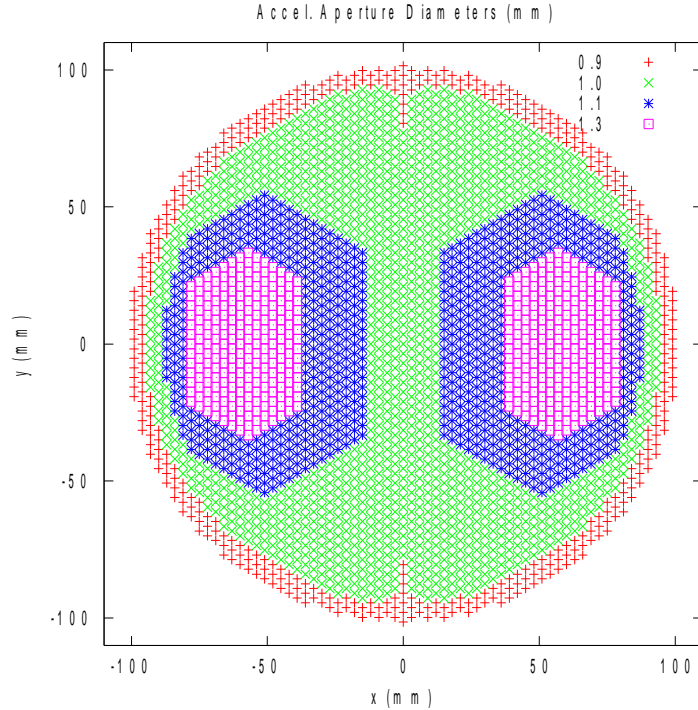


Figure 19. Aperture diameter distribution of a very Small Hole Accelerator Grid (SHAG) newly designed and fabricated. Physical open area fraction was reduced from 25% to 9%.

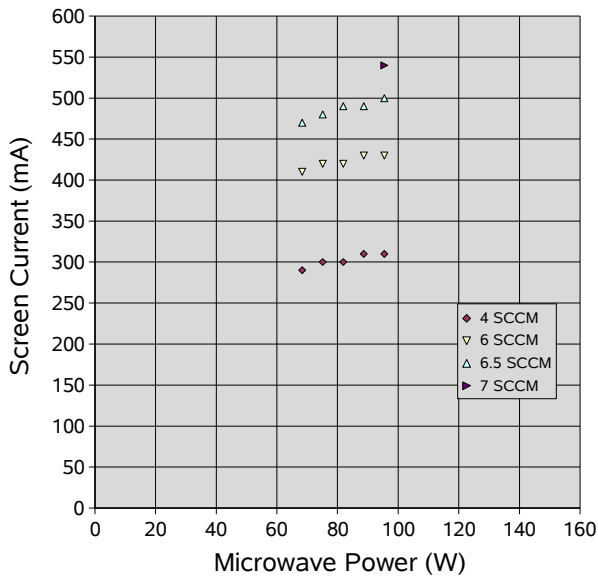


Figure 20. Screen current as a function of microwave power with the new SHAG. 6 – 10% of the screen current was the accelerator current.

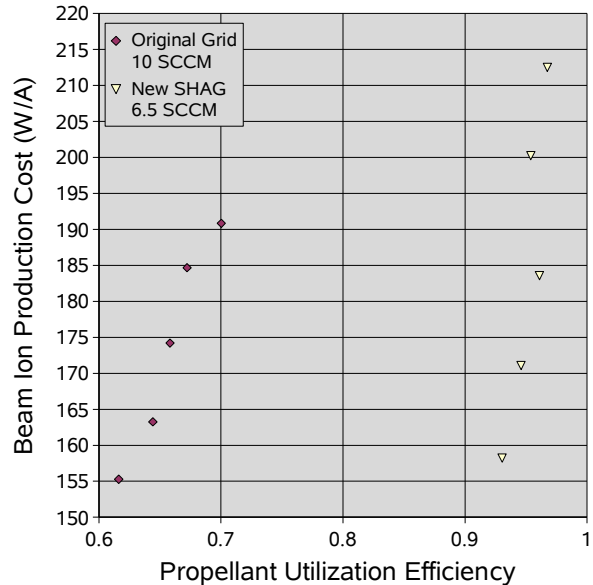


Figure 21. Preliminary propellant utilization enhancement with the new accelerator grid at microwave powers of 68 – 95 W. The performances were calculated by using screen currents subtracted by accelerator currents as beam currents. Increase of the cost is due to the severe direct impingement.

IV. Conclusion

Two-dimensional microwave E-field distributions inside the discharge chamber under beam extraction and beam profiles 5-cm downstream the ion optics have been measured. The thruster performance is much better when the distributions were quite non-uniform. Improvement of the propellant utilization efficiency using an ion machined small hole accelerator grid is ongoing effort.

References

- ¹Nishiyama, K., Nakai, T. and Kuninaka, H., "Performance Improvement of the Microwave Discharge Ion Thruster $\mu 20$," *AIAA Joint Propulsion Conference*, AIAA-2006-5176, July 2006.
- ²Nishiyama, K. and Kuninaka, H., "20-cm ECR plasma generator for xenon ion propulsion," *Thin Solid Films*, Vol. 506-507, 2006, pp. 588 – 591.
- ³Arakawa, Y. and Ishihara, K., "A Numerical Code for Cusped Ion Thrusters," *Proceedings of 22nd International Electric Propulsion Conference*, Viareggio, Italy, IEPC-91-118, 1991.
- ⁴Hudson, W. R., "Auxiliary Propulsion Thruster Performance with Ion Machined Accelerator Grids," *AIAA 11th Electric Propulsion Conference*, AIAA-1975-425, March 1975.